FUNCTIONAL
MATERIALS

Silicate apatite phosphors for pc-LED applications

Marco Kirm[a], Eduard Feldbach[a], Henri Mägi[a], Vitali Nagirnyi[a], Eliko Tõldsepp[a], Sebastian Vielhauer[a], Thomas Jüstel[b], Thomas Jansen[b], Nikolai M. Khaidukov[c], and Vladimir N. Makhov[d*]

[a] Institute of Physics, University of Tartu, W. Ostwald Str. 1, 50411 Tartu, Estonia
[b] Münster University of Applied Sciences, Stegerwaldstrasse 39, 48565 Steinfurt, Germany
[c] N. S. Kurnakov Institute of General and Inorganic Chemistry, Leninskiy Prospekt 31, 119991 Moscow, Russia
[d] P. N. Lebedev Physical Institute, Leninskiy Prospekt 53, 119991 Moscow, Russia

Abstract. Single-phase ceramic samples of silicate apatites $M_2Ln_8(SiO_4)_6O_2$ (M = Mg, Ca, Sr; Ln = Y, La) undoped and doped with Eu^{3+}, Ce^{3+}, or Mn^{2+} ions were obtained by the high-temperature solid-state reaction technique using precursors synthesized under hydrothermal conditions. The phosphors were characterized by XRD analysis, Raman spectroscopy, and steady-state/time-resolved and site-selective photoluminescence spectroscopy under blue-to-VUV excitation. It is shown that the small-radius Mg^{2+} ions, which can occupy two types of suitable sites in the apatite structure, strongly influence luminescence properties of apatites, in particular the distribution of Eu^{3+} ions between these sites. A bright broad-band yellow emission (peaked at 560 nm with $\tau < 1$ μs) was obtained from the $Mg_2La_8(SiO_4)_6O_2$:Eu apatite after annealing it in a $H_2(15\%)/Ar$ reducing atmosphere. This emission is due to 5d–4f transitions of Eu^{2+} and is efficiently excited by near UV-to-blue light (300–450 nm). Silicate apatites co-doped with optimal concentrations of Eu^{3+}/Eu^{2+} or Eu^{2+}/Mn^{2+} can be considered as possible single-phase phosphors for application in warm white pc-LEDs.

Key words: optical materials; luminescence of Eu^{3+}, Eu^{2+}, Ce^{3+}, Mn^{2+}; silicate apatites; pc-LED.

1. INTRODUCTION

Development of new highly efficient phosphors for white light generation using light emitting diodes (LEDs) is presently one of the most important topics for the creation of light sources for general and special lighting. LED-driven light sources offer significant advantages compared to other lighting technologies, namely low power consumption, high efficiency, long service life, compact size, environmentally-friendly (mercury-free) modules, and high resistance to external conditions [1–7]. LED-based sources of white light comprise phosphors

for the conversion of the primary radiation emitted by the semiconductor into light of different colours. For the designation of such light sources the term phosphor-converted LEDs (pc-LEDs) is commonly used.

There are two main approaches to making pc-LEDs emitting white light. One type of white pc-LEDs consists of the combination of a blue emitting LED chip with a yellow emitting phosphor, such as Ce^{3+} doped yttrium aluminium garnet $Y_3Al_5O_{12}$:Ce (YAG:Ce). Such pc-LED sources generate white light due to colour mixing of blue radiation from the LED chip with yellow luminescence of Ce^{3+} ions, which is due to interconfigurational 5d–4f transitions. The requirement to enable efficient absorption of blue light emitted by the LED

---

[*] Corresponding author, makhov@sci.lebedev.ru

restricts the choice of suitable doping ions mainly to Ce^{3+} and Eu^{2+}, while Mn^{4+} is regarded as an alternative ion for deep red emission, even though its absorption cross-section is much lower. The focus of LED research activities is on Ce^{3+} and Eu^{2+} due to their parity- and spin-allowed f–d/d–f transitions. However, such pc-LED sources emit bluish 'cool' white light with a high correlated colour temperature and a low colour rendering index because of the deficiency of the red spectral component. For obtaining a warm white light, well adjusted for human eyes, i.e. having a high colour rendering index and the required correlated colour temperature, a red emitting phosphor should be added to the above combination.

The other approach to making white pc-LEDs is based on using near UV emitting LEDs in the combination with a blend of blue, green, and red emitting phosphors. A widely discussed solution could be a single-phase phosphor emitting luminescence bands of different colours due to the presence of several optically active doping ions. In order to improve the performance of warm white pc-LEDs, new efficient phosphors providing different colours, in particular, broad-band yellow-emitting and narrow-band red-emitting phosphors, are highly demanded. An interesting example could be a phosphor containing both Eu^{2+} and Eu^{3+} ions emitting broad-band yellow and narrow-line red luminescence due to Eu^{2+} interconfigurational 5d–4f and Eu^{3+} intraconfigurational 4f–4f transitions, respectively. One more option is a phosphor co-doped with yellow-emitting Eu^{2+} and red-emitting Mn^{2+} ions. In both embodiments an efficient energy transfer between the ions is necessary to obtain proper luminescence from both activator ions.

Silicate apatites are well-known hosts for highly-efficient, stable phosphors because of the peculiarities of their diverse crystal structure and good physical and chemical stability [8–14]. Within the crystal structure of silicate apatites (Fig. 1), having the crystal chemical formula $^{IX}A1_4{}^{VII}A2_6(SiO_4)_6O_2$ [15], the alkaline earth $(M^{2+})_2$ and rare earth $(Ln^{3+})_8$ ions can occupy two crystallographic sites in the apatite structure: a 9-co-ordinated site A1 (4f) and a 7-coordinated site A2 (6h). Owing to the presence of two types of sites for doping ions of different valence states, advanced material engineering is possible. A specific feature of the apatite crystal structure is the presence of so-called free oxygen (O4), which does not belong to any silicon tetrahedron, is closely spaced to the A2 cation, and has a charge strongly undercompensated by adjacent cations. This led to the appearance of the following principle of the site occupation in silicate apatites, formulated by Blasse [16]: it is very unfavourable to have in A2 sites cations with a large radius and a low charge.

In the present work, ceramic samples of silicate apatites $M_2Ln_8(SiO_4)_6O_2$ (M = Mg, Ca, Sr; Ln = Y, La) undoped and doped with Eu^{3+}, Ce^{3+}, or Mn^{2+} ions were synthesized and characterized by X-ray diffraction (XRD) analysis, Raman spectroscopy, and steady-state/time-resolved and site-selective photoluminescence (PL) spectroscopy under blue-to-VUV excitation. Some Eu^{3+} doped samples were annealed in a H_2/Ar reducing atmosphere in order to convert Eu^{3+} into Eu^{2+}. The
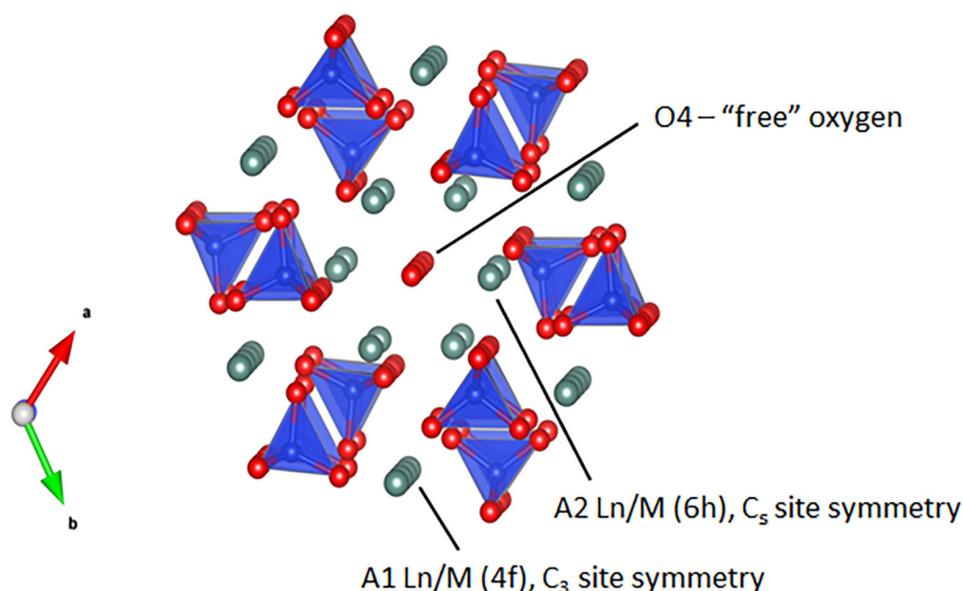

Fig. 1. Crystal structure of apatites $M_2Ln_8Si_6O_{26}$ (M = Mg, Ca, Sr; Ln = Y, La).

electronic and luminescence properties of synthesized apatites are compared with regard to their phosphor composition and synthesis conditions, and the apatites are discussed as possible phosphors for pc-LED applications.

2. EXPERIMENTAL

Ceramic samples of silicate apatites $M_2Ln_8(SiO_4)_6O_2$ (M = Mg, Ca, Sr; Ln = Y, La) undoped and doped with Eu^{3+} (0.5, 1.0, and 2.0 at.%), Ce^{3+} (0.5 at.%) or Mn^{2+} (1.0 at%) were synthesized by a high-temperature solid-state reaction at 1300 °C for 10 h upon using precursors obtained under hydrothermal conditions [17]. Some as-synthesized samples were annealed in a $H_2(15\%)/Ar$ reducing atmosphere (1200 °C, 5 h) in order to convert Eu^{3+} into Eu^{2+}. Each ceramic sample was ground into a finely dispersed powder before annealing and pressed into a tablet after the procedure.

Powder XRD patterns were obtained using a Bruker D8 Advance X-Ray powder diffractometer with Cu K_α radiation. Identification of synthesized compounds, indexing of X-ray powder diffraction patterns, and refinement of unit-cell parameters were performed with the Diffrac.Suite.EVA software (Bruker).

The vibrational spectra of silicate apatite samples were recorded using a Renishaw inVia micro-Raman spectrometer under 488 nm laser radiation at room temperature as described earlier [18].

Particle size and morphology were investigated by using scanning electron microscopy (SEM). For this purpose, a scanning electron microscope Zeiss EVO MA10 equipped with a LaB_6-cathode was used. The pressure in the sample chamber was 5×10^{-5} Pa and the acceleration voltage was 20 kV. For morphological investigation the obtained ceramics were ground into fine powders.

The PL and PL excitation (PLE) spectra were mostly recorded on an Edinburgh Instruments FSL900 spectrometer equipped with a Xenon arc lamp (450 W) and a cooled (–20 °C) single-photon counting photomultiplier (Hamamatsu R2658P). Spectral resolution for PL and PLE spectra measurements was typically set to 0.1 nm. The obtained PL spectra were corrected by applying a spectral sensitivity function obtained from a tungsten incandescent lamp certified by the National Physics Laboratory, United Kingdom.

The luminescence of undoped samples under excitation in the UV/VUV spectral range was studied using a VUV spectrometer set-up equipped with a 150 W Hamamatsu deuterium lamp and McPherson Model 302 VUV monochromator for excitation. Samples were mounted on an ARS closed-cycle helium cryostat covering a temperature range from 5.5 to 400 K, and PL

was recorded using a Shamrock 303i spectrometer in combination with a Hamamatsu 8295-01 photon counting head. Excitation spectra were normalized using sodium salicylate luminescence for reference [19].

Some spectral measurements were performed using a self-assembled set-up consisting of a deuterium 400 W discharge lamp DDS-400 and a double-quartz prism monochromator DMR-4 (Russia) in the excitation channel. The luminescence was analysed using an ARC SpectraPro 2300i grating spectrometer equipped with a position sensitive CCD camera (Princeton Instruments) and a Hamamatsu H6240-01 photon counting head as detectors in two normal channels (see also [19] for experimental details).

Time-dependent PL measurements upon 260 nm and 273 nm excitation were recorded by using a microsecond pulsed Xe flash lamp attached to an Edinburgh Instruments FSL900 spectrometer. Some measurements of emission decay kinetics were performed also with a Perkin-Elmer FX-1152 Flashtube (pulse duration 1 μs) and an Ortec MCS-PCI Card with 100 ns time resolution [20] in combination with the above-described self-assembled set-up.

Temperature-dependent PL measurements from 80 to 500 K were performed using an Oxford Instruments cryostat MicrostatN2. Liquid nitrogen was used as the cooling agent. The temperature stabilization time was 60 s and tolerance was set at ±3 K. The PL measurements at 3 K were performed using a closed-cycle cryo cooler Optistat AC-V12 from Oxford Instruments, where helium was used as the cooling agent.

3. RESULTS AND DISCUSSION

A number of ceramic samples of silicate apatites having the typical size and shape as shown in Fig. 2 were synthesized. The SEM images of synthesized ceramics
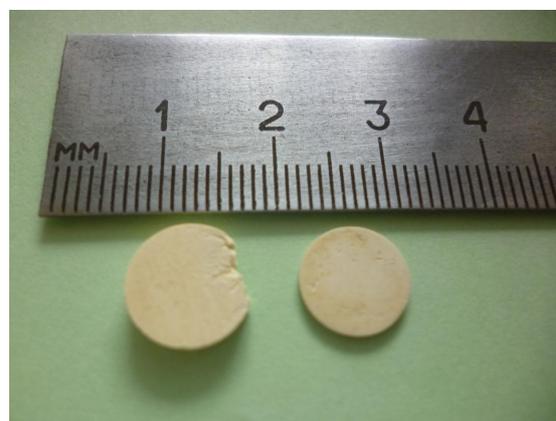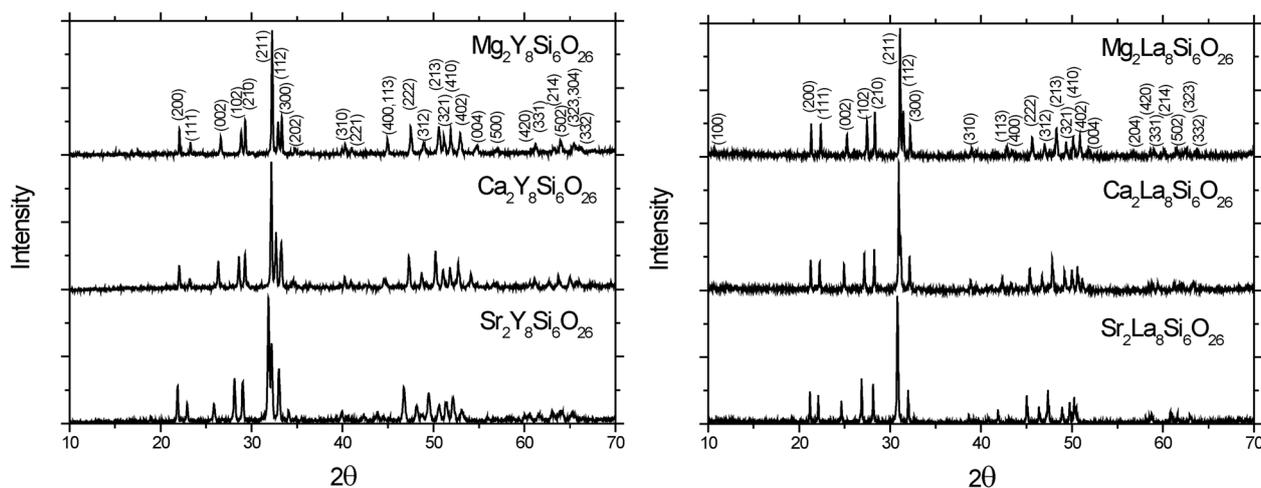

Fig. 2. Ceramic samples of silicate apatites.

Fig. 3. XRD patterns of apatites $M_2Ln_8Si_6O_{26}$ (M = Mg, Ca, Sr; Ln = Y, La).

showed that the size of particles in the ceramics was in the micron range and ceramics had a rather homogeneous macro structure.

The X-ray phase analysis confirmed that all the synthesized compounds were single-phase samples containing only apatite phases, and no reflections corresponding to any impurity were detected (Fig. 3). The XRD patterns were indexed with hexagonal cells having the lattice parameters summarized in Table 1. There was an increment of the cell parameters with ionic radii of alkaline earth element as expected whereas the change of the a/c ratio can show that there was also redistribution of ions on the sites A1 and A2 depending on the kind of the alkaline earth element. Following the above-mentioned criterion of site occupation, one can assume that, in contrast to Ca^{2+} and Sr^{2+} ions, Mg^{2+} ions having a smaller ionic radius than Ca^{2+}, Sr^{2+}, Y^{3+}, and La^{3+} ions (see Table 2) can occupy A2-type sites, which can result in different luminescence properties of Mg-apatites compared to Ca- and Sr-ones.

Some information about the electronic structure of host materials can be obtained from the studies of luminescence properties of undoped samples. As can

Table 1. Lattice parameters of apatites

	a (Å)	c (Å)	V (Å^3)	a/c
$Mg_2Y_8Si_6O_{26}$	9.317	6.705	504.1	1.39
$Ca_2Y_8Si_6O_{26}$	9.329	6.771	510.4	1.38
$Sr_2Y_8Si_6O_{26}$	9.390	6.871	524.7	1.37
$Mg_2La_8Si_6O_{26}$	9.619	7.048	564.8	1.36
$Ca_2La_8Si_6O_{26}$	9.646	7.140	575.4	1.35
$Sr_2La_8Si_6O_{26}$	9.692	7.224	587.7	1.34

Table 2. Radii of ions relevant to this research [21]

Element	Ion charge	Ionic radii, Å	
		CN = 7	CN = 9
Y	3+	0.96	1.075
La	3+	1.1	1.216
Mg	2+	0.80*	0.95*
Ca	2+	1.06	1.18
Sr	2+	1.21	1.31
Eu	3+	0.945	1.062
Eu	2+	1.20	1.30
Ce	3+	1.07	1.196
Mn	2+	0.90	1.045*

* Estimation using linear approximation.

be seen in Fig. 4, for Ca- and Sr-apatites two broad overlapping bands are observed under excitation at photon energies larger than ~5 eV. The emission band at 380 nm with the excitation band at 5.6 eV can be ascribed to the luminescence of some unidentified defects. The luminescence at 450 nm excited in the region near the edge of the intrinsic absorption of the host material, whose intensity is strongly increased at low temperature, can be attributed to excitonic emission (luminescence of self-trapped excitons or near-defect self-trapped excitons). The band gap energy can be estimated by the value ~7.6 eV where the excitation efficiency of excitonic luminescence strongly decreases. This value correlates with data of [14]. The luminescence properties of undoped Ca- and Sr-apatites are very similar, whereas Mg-apatite showed only one intense broad luminescence band, which looks similar to the luminescence ascribed to the excitonic luminescence in Ca- and Sr-based apatites.
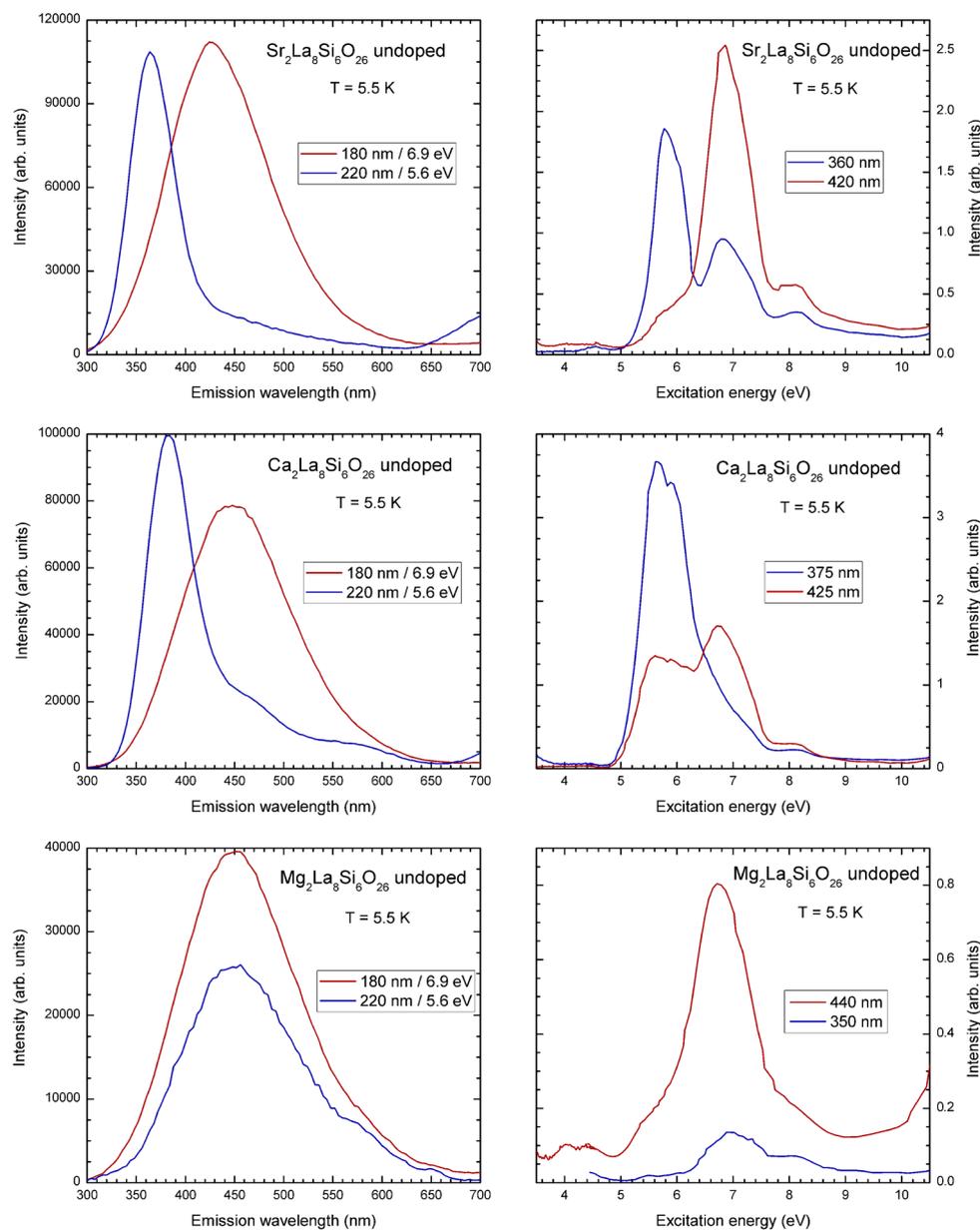
Fig. 4. Emission (left column) and excitation (right column) spectra of undoped apatites $M_2La_8Si_6O_{26}$ (M = Mg, Ca, Sr) at 5.5 K.

In order to reveal the site occupation by Eu^{3+} ions depending on the type of the alkaline earth cation in the host composition, site-selective spectroscopy studies were performed for the series of Eu^{3+} doped silicate apatites $M_2Y_8(SiO_4)_6O_2$ (M = Mg, Ca, Sr) [22]. Generally speaking, this is a well-known method for the identification of high-resolution fluorescence spectra originating from 4f–4f transitions of Eu^{3+} at different crystallographic sites (see, e.g. [23–27]). The PL and PLE spectra of all three samples show the typical behaviour for Eu^{3+} ions in oxide hosts: a broad charge-transfer (CT) excitation band (around 270 nm) and several groups of lines in

PL and PLE spectra corresponding to different 4f–4f transitions of Eu^{3+} (see Fig. 5a for the $Ca_2Y_8(SiO_4)_6O_2:Eu^{3+}$ apatite as an example). The respective groups of lines in PLE spectra are located at about 578 nm ($^7F_0$–$^5D_0$ transitions), at about 535 nm ($^7F_0$–$^5D_1$ transitions), at about 465 nm ($^7F_0$–$^5D_2$ transitions), and at about 395 nm ($^7F_0$–$^5D_3$, $^5L_6$ transitions). Emission lines between 580 and 720 nm in PL spectra correspond to the $^5D_0$–^7F_J (J = 0, 1, 2, 3, 4) transitions of Eu^{3+}. The number of Stark levels for each multiplet term ^7F_J differs for the site A1, having C_3 site symmetry, and site A2, which possesses C_s site symmetry. For J = 0, 1, 2, the number
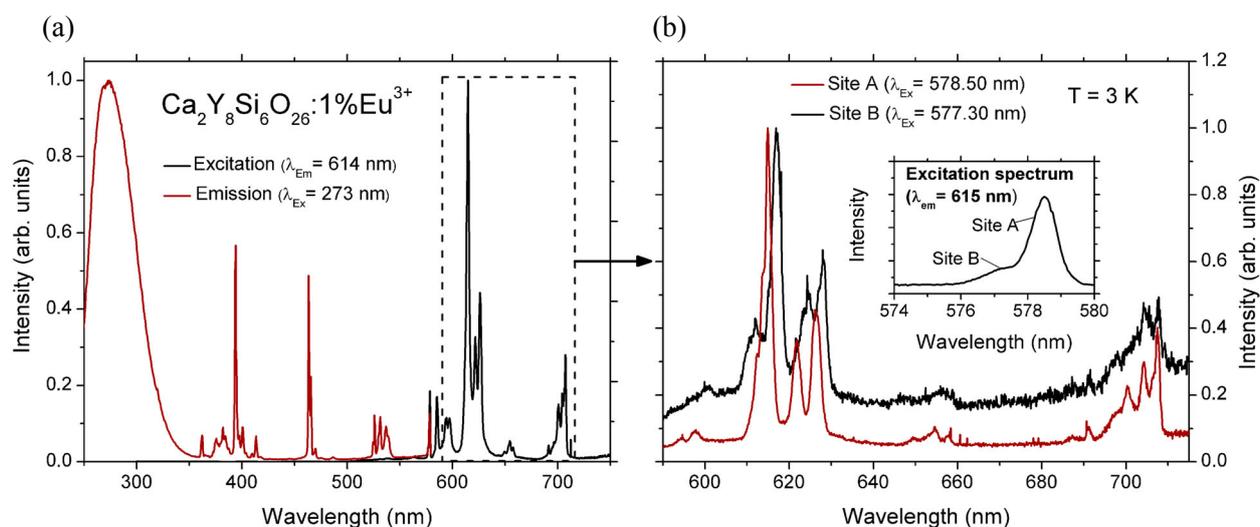
(a)   (b)

Fig. 5. (a) Emission and excitation spectra of $Ca_2Y_8Si_6O_{26}$:Eu^{3+} at 3 K; (b) site-selective emission spectra of $Ca_2Y_8Si_6O_{26}$:Eu^{3+} at 3 K. The inset shows the excitation spectrum in the region of the $^7F_0 - {}^5D_0$ transition for the two distinct sites (monitored $^5D_0 - {}^7F_2$ luminescence at 615 nm) [22].

of Stark levels and accordingly the maximum number of lines in the spectrum of $^5D_0 - {}^7F_J$ transitions can be 1, 2, 3, respectively, for site A1 and 1, 3, 5, respectively, for site A2.

The results of low-temperature high-resolution measurements of PLE spectra in the region of the $^7F_0 - {}^5D_0$ Eu^{3+} transitions (inset in Fig. 5b) clearly show that there are two distinct sites (marked in the figure as site A and site B) occupied by Eu^{3+} in $Ca_2Y_8Si_6O_{26}$. Also there is practically no difference for Ca- and Sr-apatites. For these two apatites, $Ca_2Y_8Si_6O_{26}$ and $Sr_2Y_8Si_6O_{26}$, the luminescence intensity of Eu^{3+} in site A is much higher than in site B, which can correlate with relative concentrations of Eu^{3+} ions occupying these two types of sites. The PL spectra recorded under site-selective excitation (Fig. 5b) show that the number of lines corresponding to $^5D_0 - {}^7F_2$ transitions of Eu^{3+} (at about 620 nm) is three for the excitation at site A and is not less than four for the excitation at site B. Thus one can assume that the spectroscopic site A corresponds to the structural A1-type site and site B to the A2-type site. Accordingly, Eu^{3+} ions enter in Ca- and Sr-based matrices preferably the A1-type sites. On the other hand, in Mg-apatite the luminescence intensities for the two sites are roughly equal. This indicates that a large part of Eu^{3+} ions in the Mg-based matrix reside in the A2 sites. The energy of the CT band, which is strongly influenced by the crystal field strength, is different for two sites, and as expected, the higher energy corresponds to Eu^{3+} ions at the A1 sites, which have the larger coordination number.

Time-dependent luminescence measurements show a bi-exponential decay behaviour for each investigated

Eu^{3+} doped apatite, which can be explained by the two distinct sites occupied by Eu^{3+} within the apatite structure (see Fig. 6 for the $Mg_2Y_8Si_6O_{26}$:Eu^{3+} apatite as an example). The parameters of bi-exponential decay for three apatites are listed in Table 3. It can be assumed that the decay component with a longer lifetime, which has a larger weight, corresponds to the luminescence of Eu^{3+} occupying the A1 sites in accordance with relative intensities of luminescence obtained in site-selective spectra from the two sites for Sr- and Ca-apatites. On the other hand, for Mg-apatite the intensities of the two components are comparable. This result again points to the approximately equal population of A1 and A2 sites by Eu^{3+} ions in this apatite, similar to results of site-selective spectra measurements.

The temperature-dependent measurements showed that the emission intensity integrals dropped considerably with increasing temperature up to 500 K (see Fig. 7 for the $Mg_2Y_8Si_6O_{26}$:Eu^{3+} apatite as an example). The temperature dependence of the Eu^{3+} luminescence intensity $I(T)$ can be described with the Fermi–Dirac model:

$$I(T) = \frac{I_0}{1 + B \cdot \exp\left(-\dfrac{E_A}{k_B T}\right)}, \qquad (1)$$

where I_0 is the luminescence intensity at $T = 0$ K, B characterizes the rate of thermal quenching, k_B is the Boltzmann constant, and E_A is the energy barrier (activation energy) for thermal quenching as a result of the cross-over of the emitting (Eu^{3+} $^5D_0$) state to the quenching state.

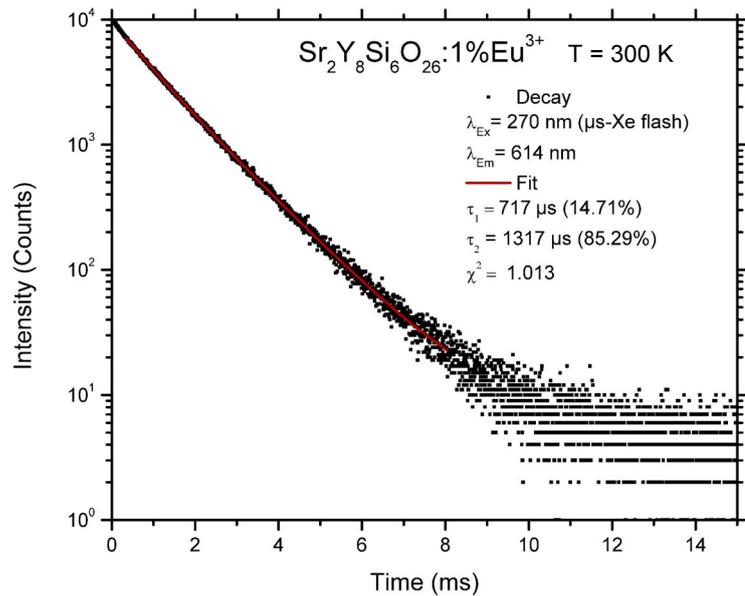$Sr_2Y_8Si_6O_{26}$:1%Eu^{3+} T = 300 K

- Decay
  λ_{Ex} = 270 nm (μs-Xe flash)
  λ_{Em} = 614 nm
— Fit
  τ_1 = 717 μs (14.71%)
  τ_2 = 1317 μs (85.29%)
  χ^2 = 1.013

Fig. 6. Luminescence decay curve of $Sr_2Y_8Si_6O_{26}$:Eu^{3+} (1%) at 300 K under excitation into the O^{2-}–Eu^{3+} CT band. The band pass for luminescence detection was 5 nm [22].

Table 3. Parameters of bi-exponential fits to the decay curves of Eu^{3+} in $M_2Y_8(SiO_4)_6O_2$ (M = Mg, Ca, Sr) [22]

M	τ_1 (μs)	τ_2 (μs)
Sr	717 (15%)	1317 (85%)
Ca	539 (10%)	1252 (90%)
Mg	931 (32%)	1428 (68%)

The values of activation energies E_A and thermal quenching temperatures $T_{1/2}$ (determined as the temperature at which the emission intensity is decreased by 50% of its maximal value), obtained for three apatites from the fits with this formula are presented in Table 4. The temperature dependence of Eu^{3+} luminescence intensity is well described by this simple formula only for Ca- and Sr-apatites. In the case of Mg-apatite a more complicated quenching behaviour is observed, which is well described by a bi-sigmoidal law (see Fig. 7). This
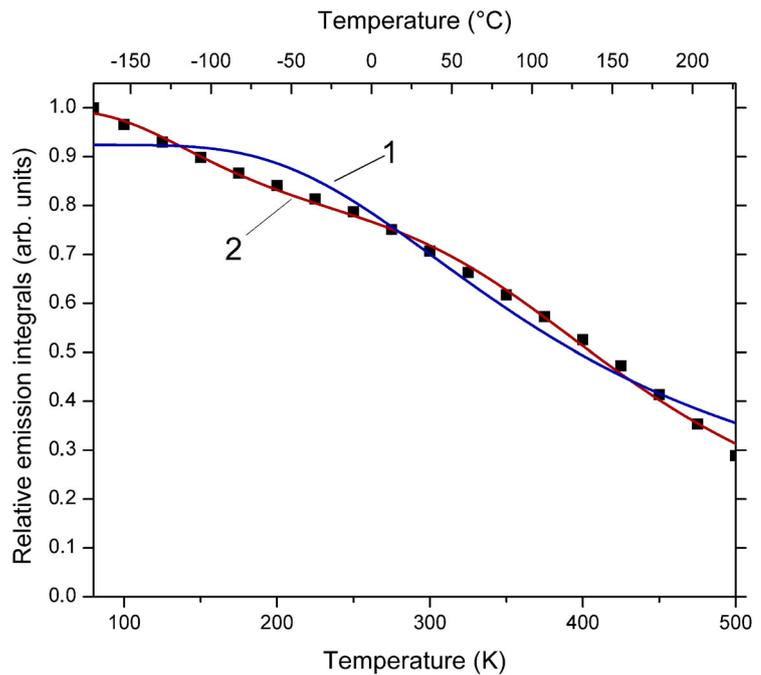

Fig. 7. Temperature dependence of Eu^{3+} photoluminescence of $Mg_2Y_8Si_6O_{26}$:Eu^{3+}: dots are experimental data, curves represent sigmoidal (1) and bi-sigmoidal (2) fit functions.

Table 4. Parameters of Eu^{3+} luminescence thermal quenching derived from Fermi–Dirac fits [22]

M	E_a (eV)	$T_{1/2}$ (K)
Sr	0.061 ± 0.008	561 ± 39
Ca	0.097 ± 0.026	591 ± 19
Mg	0.104 ± 0.011	419 ± 11

feature is due to the overlapping of luminescence from two Eu^{3+} sites that have comparable concentrations but show different temperature behaviours.

The calculated colorimetric parameters of Eu^{3+} luminescence are typical for Eu^{3+} based phosphors (Table 5), but these results demonstrate that the Mg-compound shows considerably different values of parameters compared to Ca- and Sr-hosts. In particular, the asymmetry ratio, which is usually used for the characterization of the Eu^{3+} local site symmetry, is much smaller for the Mg-apatite. This indicates again different site occupation by Eu^{3+} ions in the Mg-apatite compared to Ca- and Sr-apatites. Thus, small-radius Mg^{2+}
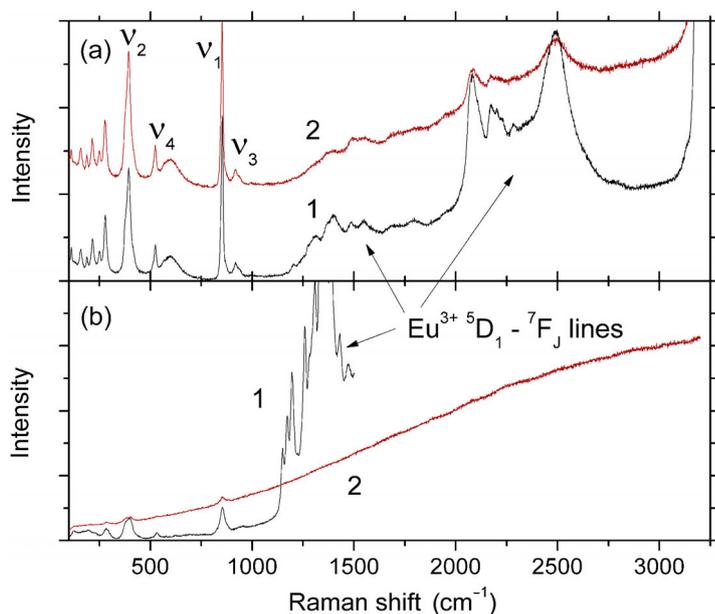
ions, which can occupy sites of both A1 and A2 types, strongly influence the properties of Eu^{3+} luminescence in apatites, in particular the distribution of Eu^{3+} ions at the sites of A1 and A2 types.

Spectroscopic studies of Eu^{3+} luminescence have been performed also for one more series of Eu^{3+} doped apatites with La ions in the matrix instead of Y: $M_2La_8Si_6O_{26}:Eu^{3+}$ (M = Mg, Ca, Sr) [28]. The PL and PLE spectra of all these samples also show the typical behaviour for Eu^{3+} ions in oxide hosts. On the other hand, according to the obtained emission spectra in the region of $^5D_0$–$^7F_2$ transitions of Eu^{3+}, one can conclude that in these apatites Eu^{3+} is mainly substituted to the A2 (6h) site with the C_s symmetry because the number of lines corresponding to these transitions is always larger than three. Under short-wavelength excitation ($\lambda < 250$ nm), a broadband emission is also observed from these samples, which is related to some intrinsic luminescence of the hosts, as discussed above.

Some apatite samples doped with Eu^{3+} were annealed in a $H_2(15\%)/Ar$ reducing atmosphere (1200 °C, 5 h) in order to convert Eu^{3+} into Eu^{2+}. Raman spectra (Fig. 8)

Table 5. Colorimetric parameters of Eu^{3+} luminescence in apatites $M_2Y_8(SiO_4)_6O_2$ (M = Mg, Ca, Sr) relevant to LED applications [22]

	$Mg_2Y_8Si_6O_{26}:Eu^{3+}$	$Ca_2Y_8Si_6O_{26}:Eu^{3+}$	$Sr_2Y_8Si_6O_{26}:Eu^{3+}$
Asymmetry ratio (610–630 nm / 590–605 nm)	5.9	8.6	9.3
Colour coordinates C.I.E. 1931	x = 0.610 y = 0.346	x = 0.639 y = 0.358	x = 0.636 y = 0.361
Luminous efficacy	293 lm/W	214 lm/W	234 lm/W

Fig. 8. Raman spectra of Eu^{3+} doped apatites $Sr_2La_8Si_6O_{26}:Eu$ (a) and $Mg_2La_8Si_6O_{26}:Eu$ (b): as-synthesized (1) and annealed in a $H_2(15\%)/Ar$ reducing atmosphere (2). $T = 300$ K.

of these samples show a well-defined characteristic structure of silicate apatites (for energies below ~1100 cm^{-1}) [29] including the peaks corresponding to the ν_1, ν_2, ν_3, and ν_4 vibration modes of the SiO$_4$ tetrahedron. However, for Mg-apatite a considerable broadening of the peaks is observed in the spectrum indicating the presence of disordering in the crystal structure. After the H$_2$/Ar treatment the Raman spectra of Ca- and Sr-apatites remained unchanged. On the other hand, under 488 nm laser excitation the H$_2$/Ar-treated Mg-apatite samples emit very bright broadband luminescence, which overlaps with the host vibration peaks. This feature prohibited recording good-quality Raman spectra for the H$_2$/Ar-treated Mg-apatite.

Luminescence spectra of Eu^{3+} doped Ca- and Sr-apatites practically do not change after the treatment in a reducing atmosphere. In contrast to that, the Mg$_2$La$_8$(SiO$_4$)$_6$O$_2$:Eu samples emit yellow luminescence as a result of such treatment (see photo in Fig. 9), which is due to an intense broad emission band centred at 560 nm (Fig. 10). This emission can be effectively excited within the UV to blue spectral region with the maximum excitation efficiency at ~370 nm, well matched with the emission of near-UV LEDs. Decay kinetics of this emission is non-exponential, but the main decay component has a decay time less than 1 μs. Due to the observed spectral and decay kinetics properties, namely overlapping broad excitation and emission bands with minimal Stokes shift, decay time < 1 μs, the yellow emission detected from Mg$_2$La$_8$(SiO$_4$)$_6$O$_2$:Eu after the H$_2$/Ar treatment can be assigned to the 5d–4f radiative transitions of Eu^{2+} ions. However, the Eu^{3+} 4f–4f emission is still observable from the reduced Mg$_2$La$_8$(SiO$_4$)$_6$O$_2$:Eu sample under excitation in the CT band spectral region.
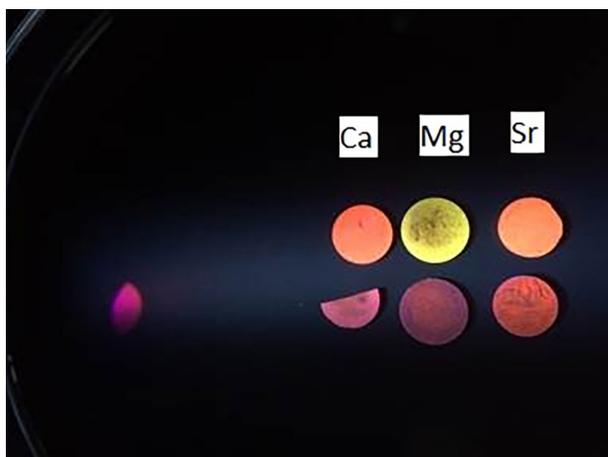

Fig. 9. Visible luminescence under UV radiation from three different Eu-doped (1.0 at.%) apatite samples: before (lower row) and after (upper row) annealing in a H$_2$/Ar atmosphere [28].

The obtained results show that an efficient Eu$^{3+} \rightarrow$ Eu^{2+} reduction is achieved only for Mg$_2$La$_8$(SiO$_4$)$_6$O$_2$:Eu^{3+}. This can originate from the specific site occupation in Mg^{2+}-apatites. In contrast to Sr^{2+} and Ca^{2+} ions residing at the A1 sites, Mg^{2+} ions with a considerably smaller ionic radius than La^{3+} tend to occupy the A2 sites, which is assisted by the appearance of oxygen vacancies at the nearby O4 positions for local charge compensation of Mg^{2+} ions. This disordering of the lattice structure can be a reason of the observed broadening of the Raman spectra for Mg-apatites. Since the Eu^{3+} ions are located also predominantly at the A2 sites, after the reducing reaction Eu$^{3+} \rightarrow$ Eu^{2+}, the Eu^{2+} ions can be stabilized by the creation of nearby oxygen vacancies due to their migration along the O4 positions at the neighbouring Mg^{2+} ions.

Obviously, the concentration of Eu^{3+} ions in this particular phosphor composition is not optimal for efficient energy transfer from Eu^{2+} to Eu^{3+} ion, and the emission spectrum does not show any red emission lines of Eu^{3+} under near-UV or blue excitation. It is observed only under CT band excitation in this sample. However, because of the good overlap of the Eu^{2+} emission band with the 4f–4f absorption lines of Eu^{3+} ions (see Fig. 10) one can expect that for an optimally chosen Eu^{3+} concentration in the synthesized apatites and by optimizing the conditions of annealing in a reducing atmosphere, the optimal ratio of Eu^{2+} and Eu^{3+} ions can be obtained for an efficient conversion of some part of the Eu^{2+} yellow luminescence into the red emission of Eu^{3+} under UV/blue excitation. Such a single-phase phosphor would be highly interesting for application in warm white pc-LEDs.

The synthesized Ce^{3+} doped silicate apatites show rather broad and structured emission bands (Fig. 11), which can be explained by the presence of at least two Ce^{3+} optical centres related to two kinds of sites in silicate apatites (see also [8,10]). Similarly to results obtained earlier for many other families of apatites, the Ce^{3+} 5d–4f luminescence spectrum lies mainly in the green spectral range and is excited in a rather deep UV region, i.e. out of the spectral range of emission for typical near-UV LEDs. In these apatites Ce^{3+} luminescence possesses also a considerable thermal quenching with a $T_{1/2}$ value near room temperature. Thus, these Ce^{3+} doped silicate apatites are not very suitable systems for pc-LED applications.

The emission and excitation spectra of Mn^{2+} luminescence obtained for Mn^{2+} doped silicate apatite Mg$_2$La$_8$Si$_6$O$_{26}$ are presented in Fig. 12. The Mn^{2+} ions emit a broad-band red luminescence at 609 nm due to ^{4}T$_1$–^{6}A$_1$ transitions excited both in the blue/green (broad band) and near-UV (narrow band) spectral range (see also [11]). Mn^{2+} luminescence shows relatively good thermal stability in this host with $T_{1/2}$ = 514 K (Fig. 13).
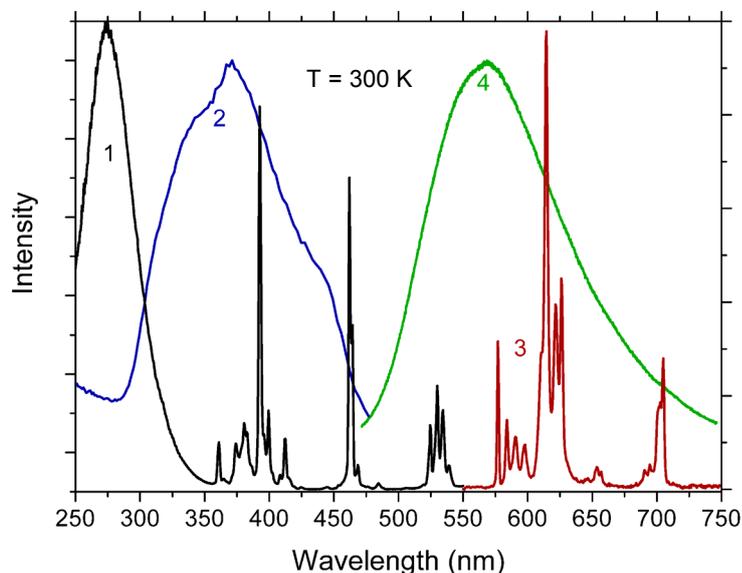
Fig. 10. Excitation spectra monitored at 614 (1) or 550 (2) nm and emission spectra under excitation at 275 (3) or 355 nm (4) of Eu^{3+} (1, 3) and Eu^{2+} (2, 4) in $Mg_2La_8Si_6O_{26}$ at 300 K [28].
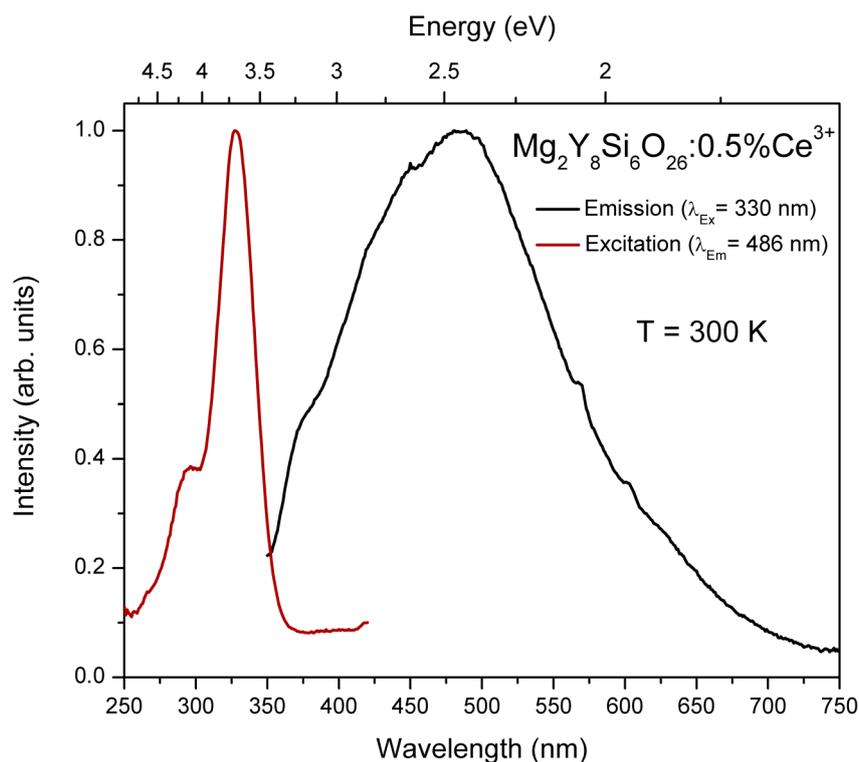

Fig. 11. Normalized excitation (monitored at 486 nm) and emission (under excitation at 330 nm) spectra of $Mg_2Y_8Si_6O_{26}$:0.5%Ce^{3+} at 300 K.

However, the respective transitions of Mn^{2+} are parity- and spin-forbidden, i.e. absorption of blue or UV excitation light by Mn^{2+} ions is very inefficient. This means that the materials singly doped with Mn^{2+} can usually not be considered as practical phosphors. For high-efficient excitation of Mn^{2+} luminescence, some sensitizer ions are needed. Such sensitizers can be Eu^{2+}

ions, whose emission spectrum well overlaps with the broad absorption band of Mn^{2+} at 500 nm caused by $^6A_1$–$^4T_2$ transitions. By choosing the proper concentrations of Eu^{2+} and Mn^{2+} ions one could expect to obtain an efficient energy transfer from Eu^{2+} to Mn^{2+}. This will provide the co-existence of yellow luminescence of Eu^{2+} and red emission of Mn^{2+} from a single-phase
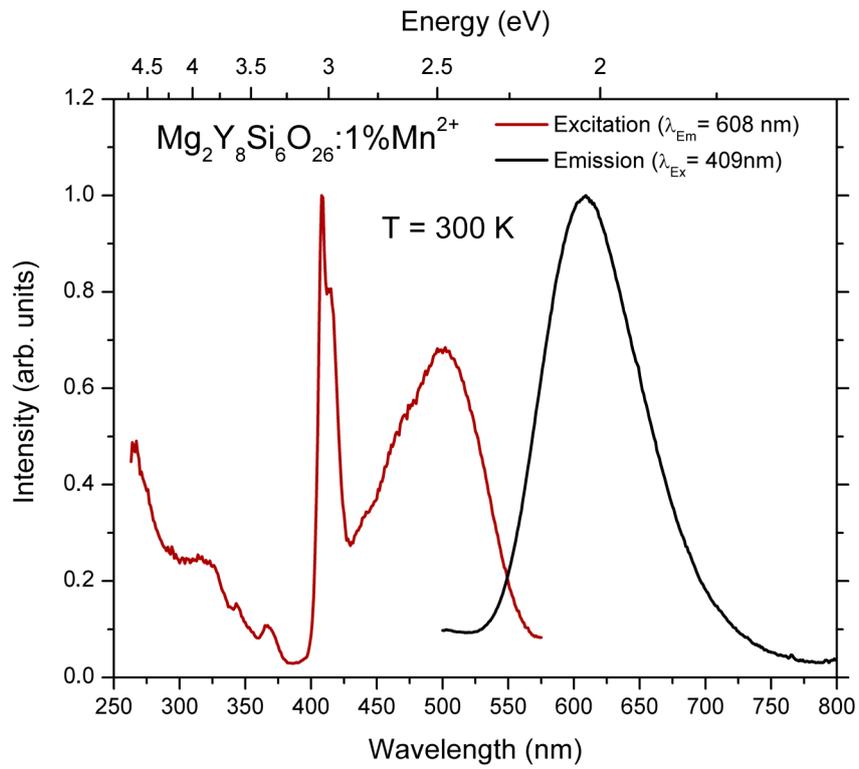
Fig. 12. Normalized excitation (monitored at 608 nm) and emission (under excitation at 409 nm) spectra of $Mg_2Y_8Si_6O_{26}$:1%Mn^{2+} at 300 K.

Fig. 13. Temperature dependence of Mn^{2+} photoluminescence from $Mg_2Y_8Si_6O_{26}$:1%Mn^{2+}.

phosphor with the resulting spectrum well corresponding to requirements for applications in warm white light pc-LED sources.

4. CONCLUSIONS

Single phase silicate apatites $M_2Ln_8Si_6O_{26}$ (M = Mg, Ca, Sr; Ln = Y, La) undoped and doped with Eu^{3+}, Ce^{3+}, or Mn^{2+} were prepared by high-temperature solid-state reaction using the precursors synthesized under hydrothermal conditions. The Mg^{2+} ions, which have a smaller ionic radius than Ca^{2+}, Sr^{2+}, Y^{3+}, and La^{3+} ions, tend to occupy the A2-type sites in the apatite lattice, which results in different luminescence properties of Mg-apatites compared to Ca- and Sr-ones. Efficient conversion of Eu^{3+} to Eu^{2+} was obtained for $Mg_2La_8(SiO_4)_6O_2{:}Eu^{3+}$ after annealing in a H_2/Ar reducing atmosphere due to the charge compensation mechanism by oxygen vacancies. Apatite $Mg_2La_8(SiO_4)_6O_2{:}Eu^{2+}$ shows a broad yellow emission band (peaked at 560 nm with $\tau < 1$ µs) due to 5d–4f transitions of Eu^{2+}, which is efficiently excited by near-UV-to-blue radiation. Silicate apatites co-doped with optimal concentrations of Eu^{3+}/Eu^{2+} or Eu^{2+}/Mn^{2+} can be considered as possible single phase phosphors for making warm white pc-LEDs.

ACKNOWLEDGEMENTS

REFERENCES

1. Feldmann, C., Jüstel, T., Ronda, C. R., and Schmidt, P. J. Inorganic luminescent materials: 100 years of research and application. *Adv. Funct. Mater.*, 2003, **13**, 511–516.

2. Schubert, E. F. and Kim, J. K. Solid-state light sources getting smart. *Science*, 2005, **308**, 1274–1278.

3. Ye, S., Xiao, F., Pan, Y. X., Ma, Y. Y., and Zhang, Q. Y. Phosphors in phosphor-converted white light-emitting diodes: recent advances in materials, techniques and properties. *Mat. Sci. Eng.*, 2010, **R 71**, 1–34.

4. Smet, P. F., Parmentier, A. B., and Poelman, D. Selecting conversion phosphors for white light-emitting diodes. *J. Electrochem. Soc.*, 2011, **158**, R37–R54.

5. Li, G., Tian, Y., Zhaoa, Y., and Lin, J. Recent progress in luminescence tuning of Ce^{3+} and Eu^{2+}-activated phosphors for pc-WLEDs. *Chem. Soc. Rev.*, 2015, **44**, 8688–8713.

6. Lin, Y.-C., Karlsson, M., and Bettinelli, M. Inorganic phosphor materials for lighting. *Top. Curr. Chem. (Z)*, 2016, **374**, 21.

7. Xia, Z. and Liu, Q. Progress in discovery and structural design of color conversion phosphors for LEDs. *Prog. Mater. Sci.*, 2016, **84**, 59–117.

8. Xiao, F., Xue, Y. N., and Zhang, Q. Y. $Y_4MgSi_3O_{13}{:}RE^{3+}$ (RE = Ce, Tb and Eu) nanophosphors for a full-color display. *Physica B*, 2010, **405**, 4445–4449.

9. Zuev, M. G., Karpov, A. M., and Shkvarin, A. S. Synthesis and spectral characteristics of $Sr_2Y_8(SiO_4)_6O_2$: Eu polycrystals. *J. Solid State Chem.*, 2011, **184**, 52–58.

10. Shen, Y., Chen, R., Gurzadyan, G. G., Xu, J., Sun, H., Khor, K. A., and Dong, Z. Synthesis and spectroscopic investigations of $Sr_2Y_8(SiO_4)_6O_2$: Eu^{2+},Eu^{3+} phosphor for white LEDs. *Opt. Mater.*, 2012, **34**, 1155–1160.

11. Hsu, C.-H., Das, S., and Lu, C.-H. Color-tunable, single phased $MgY_4Si_3O_{13}$: Ce^{3+}, Mn^{2+} phosphors with efficient energy transfer for white-light-emitting diodes. *J. Electrochem. Soc.*, 2012, **159**, J193–J199.

12. Sokolnicki, J. and Zych, E. Synthesis and spectroscopic investigations of $Sr_2Y_8(SiO_4)_6O_2$: Eu^{2+},Eu^{3+} phosphor for white LEDs. *J. Lumin.*, 2015, **158**, 65–69.

13. Yuan, S., Wang, L., Cui, Z., Yang, Y., Zeng, H., Cheviré, F., et al. Color-tunable Eu^{2+} activated oxysilicate phosphors with oxyapatite structure. *J. Mater. Sci. & Appl.*, 2015, **1**, 33–37.

14. Dobrowolska, A., Karsu, E. C., Bos, A. J. J., and Dorenbos, P. Spectroscopy, thermoluminescence and afterglow studies of $CaLa_4(SiO_4)_3O$: Ln (Ln=Ce, Nd, Eu, Tb, Dy). *J. Lumin.*, 2015, **160**, 321–327.

15. Leu, L.-C., Thomas, S., Sebastian, M. T., Zdzieszynski, S., Misture, S., and Ubic, R. Crystal structure of apatite type rare-earth silicate $(Sr_2RE_2)(RE_6)(SiO_4)_6O_2$ (RE=La, Pr, Tb, Tm, and Y). *J. Am. Ceram. Soc.*, 2011, **94**, 2625–2632.

16. Blasse, G. Influence of local charge compensation on site occupation and luminescence of apatites. *J. Solid State Chem.*, 1975, **14**, 181–184.

17. Jang, K. H., Khaidukov, N. M., Tuyen, V. P., Kim, S. I., Yu, Y. M., and Seo, H. J. Luminescence properties and crystallographic sites for Eu^{3+} ions in fluorthalenite $Y_3Si_3O_{10}F$. *J. Alloys Compd.*, 2012, **536**, 47–51.

18. Omelkov, S. I., Kiisk, V., Sildos, I., Kirm, M., Nagirnyi, V., Pustovarov, V. A., et al. The luminescence microspectroscopy of Pr^{3+}-doped $LiBaAlF_6$ and $Ba_3Al_2F_{12}$ crystals. *Radiat. Meas.*, 2013, 56, 49–53.

19. Romet, I., Buryi, M., Corradi, G., Feldbach, E., Laguta, V., Tichy-Racs, E., and Nagirnyi, V. Recombination luminescence and EPR of Mn doped $Li_2B_4O_7$ single crystals. *Opt. Mater.*, 2017, **70**, 184–193.

20. Nagirnyi, V., Kotlov, A., Jönsson, L., Kirm, M., and Lushchik, A. Emission decay kinetics in a $CaWO_4$:Bi crystal. *Nucl. Instrum. Methods A*, 2005, **537**, 61–65.

21. Shannon, R. D. Revised effective ionic radii and systematic studies of interatomic distances in halides and chalcogenides. *Acta Crystallographica A*, 1976, **32**, 751–767.

22. Jansen, T., Jüstel, T., Kirm, M., Mägi, H., Nagirnyi, V., Tõldsepp, E., et al. Site selective, time and temperature dependent spectroscopy of Eu^{3+} doped apatites $(Mg,Ca,Sr)_2Y_8Si_6O_{26}$. *J. Lumin.*, 2017, **186**, 205–211.

23. Gupta, S. K., Mohapatra, M., Kaity, S., Natarajan, V., and Godbole, S. V. Structure and site selective luminescence of sol–gel derived Eu: Sr_2SiO_4. *J. Lumin.*, 2012, **132**, 1329–1338.

24. Ternane, R., Ferid, M., Panczer, G., Trabelsi-Ayadi, M., and Boulon, G. Site-selective spectroscopy of Eu^{3+}-doped orthorhombic lanthanum and monoclinic yttrium polyphosphates. *Opt. Mater.*, 2005, **27**, 1832–1838.

25. Wright, A. O., Seltzer, M. D., Gruber, J. B., and Chai, B. H. T. Site-selective spectroscopy and determination of energy levels in Eu^{3+}-doped strontium fluorophosphate. *J. Appl. Phys.*, 1995, **78**, 2456.

26. Wu, L., Tian, X., Deng, K., Liu, G., and Yin, M. Site selective spectroscopic study of an efficient red-emitting phosphor Y_2MoO_6: Eu. *Opt. Mater.*, 2015, **45**, 28–31.

27. Fiaczyk, K. and Zych, E. On peculiarities of Eu^{3+} and Eu^{2+} luminescence in Sr_2GeO_4 host. *RSC Advances*, 2016, **6**, 91836–91845.

28. Khaidukov, N. M., Kirm, M., Feldbach, E., Mägi, H., Nagirnyi, V., Tõldsepp, E., et al. Luminescence properties of silicate apatite phosphors $M_2La_8Si_6O_{26}$:Eu (M = Mg, Ca, Sr). *J. Lumin.*, 2017, **191**, Part A, 51–55.

29. Orera, A., Kendrick, E., Apperley, D. C., Orera, V. M., and Slater, P. R. Effect of oxygen content on the ^{29}Si NMR, Raman spectra and oxide ion conductivity of the apatite series, $La_{8+x}Sr_{2-x}(SiO_4)_6O_{2+x/2}$. *Dalton Trans.*, 2008, **39**, 5296–5301.

Silikaatapatiitfosfoorid rakendusteks fosfoorkonverteeritud valgusdioodides

Marco Kirm, Eduard Feldbach, Henri Mägi, Vitali Nagirnyi, Eliko Tõldsepp, Sebastian Vielhauer, Thomas Jüstel, Thomas Jansen, Nikolai M. Khaidukov ja Vladimir N. Makhov

Eu^{3+}, Ce^{3+} või Mn^{2+} ioonidega lisandatud faasipuhtad keraamilised silikaatapatiidid $M_2Ln_8(SiO_4)_6O_2$ (M = Mg, Ca, Sr; Ln = Y, La) valmistati kõrgetemperatuurilise tahkefaasi reaktsiooni meetodil, kasutades hüdrotermaalsetes tingimustes sünteesitud lähteaineid. Saadud fosfooride omaduste määramiseks kasutati XRD-analüüsi, ramanspektroskoopiat, statsionaarset ja ajalise lahutusega kohatundlikku fotoluminestsentsspektroskoopiat, ergastades sinises kuni vaakumultravioletses spektraalpiirkonnas. Näidati, et väikese raadiusega Mg^{2+} ioonid, mis võivad paigutuda kahte neile sobivasse võresõlme apatiidi struktuuris, mõjutavad Eu^{3+} ioonide jaotust nendes võresõlmedes ja seeläbi märgatavalt apatiitide luminestsentsomadusi. Peale $Mg_2La_8(SiO_4)_6O_2$:Eu apatiidi lõõmutamist redutseerivas H_2(15%)/Ar atmosfääris leiti intensiivne laiaribaline kollane kiirgus maksimumiga 560 nm ja elueaga $\tau < 1$ μs. See kiirgus on põhjustatud 5d–4f üleminekutest Eu^{2+} ioonides ja seda saab efektiivselt ergastada UV- ning sinise kiirgusega (300–450 nm). Optimaalse lisandite sisaldusega Eu^{3+}/Eu^{2+} või Eu^{2+}/Mn^{2+} dopeeritud silikaatapatiitidel on potentsiaali faasipuhaste fosfooridena rakendusteks fosfoorkonverteeritud valgusdioodides (pc-LED).